Wide-field fluorescence lifetime imaging of cancer

James McGinty,[1] Neil P. Galletly,[2] Chris Dunsby,[1,2,*] Ian Munro,[1] Daniel S. Elson,[1] Jose Requejo-Isidro,[1] Patrizia Cohen,[2] Raida Ahmad,[2] Amanda Forsyth,[2] Andrew V. Thillainayagam,[3] Mark A. A. Neil,[1] Paul M. W. French,[1] and Gordon W Stamp[2]

[1]*Photonics Group, Department of Physics, Imperial College London, South Kensington Campus, London, SW7 2AZ, UK*
[2]*Department of Histopathology, Imperial College London, Du Cane Road, London, W12 0NN, UK*
[3]*Department of Gastroenterology, Division of Medicine, Imperial College London, Hammersmith Hospital Campus, London, W12 0NN, UK*
**christopher.dunsby@imperial.ac.uk*

Abstract: Optical imaging of tissue autofluorescence has the potential to provide rapid label-free screening and detection of surface tumors for clinical applications, including when combined with endoscopy. Quantitative imaging of intensity-based contrast is notoriously difficult and spectrally resolved imaging does not always provide sufficient contrast. We demonstrate that fluorescence lifetime imaging (FLIM) applied to intrinsic tissue autofluorescence can directly contrast a range of surface tissue tumors, including in gastrointestinal tissues, using compact, clinically deployable instrumentation achieving wide-field fluorescence lifetime images of unprecedented clarity. Statistically significant contrast is observed between cancerous and healthy colon tissue for FLIM with excitation at 355 nm. To illustrate the clinical potential, wide-field fluorescence lifetime images of unstained *ex vivo* tissue have been acquired at near video rate, which is an important step towards real-time FLIM for diagnostic and interoperative imaging, including for screening and image-guided biopsy applications.

OCIS codes: (170.3650) Lifetime-based sensing; (170.3880) Medical and biological imaging.

References and links

1. S. Andersson-Engels, A. Elner, J. Johansson, S.-E. Karlsson, L. G. Salford, L.-G. Strömblad, K. Svanberg, and S. Svanberg, "Clinical Recording of Laser-induced Fluorescence Spectra for Evaluation of Tumour Demarcation Feasibility in Selected Clinical Specialities," Lasers Med. Sci. **6**(4), 415–424 (1991).
2. K. Sokolov, M. Follen, and R. Richards-Kortum, "Optical spectroscopy for detection of neoplasia," Curr. Opin. Chem. Biol. **6**(5), 651–658 (2002).
3. I. J. Bigio, and J. R. Mourant, "Ultraviolet and visible spectroscopies for tissue diagnostics: fluorescence spectroscopy and elastic-scattering spectroscopy," Phys. Med. Biol. **42**(5), 803–814 (1997).
4. R. Richards-Kortum, and E. Sevick-Muraca, "Quantitative optical spectroscopy for tissue diagnosis," Annu. Rev. Phys. Chem. **47**(1), 555–606 (1996).
5. G. A. Wagnières, W. M. Star, and B. C. Wilson, "In vivo fluorescence spectroscopy and imaging for oncological applications," Photochem. Photobiol. **68**(5), 603–632 (1998).
6. K. Gono, K. Yamazaki, N. Doguchi, T. Nonami, T. Obi, M. Yamaguchi, N. Ohyama, H. Machida, Y. Sano, S. Yoshida, Y. Hamamoto, and T. Endo, "Endoscopic observation of tissue by narrowband illumination," Opt. Rev. **10**(4), 211–215 (2003).
7. W. L. Curvers, F. J. C. van den Broek, J. B. Reitsma, E. Dekker, and J. J. Bergman, "Systematic review of narrow-band imaging for the detection and differentiation of abnormalities in the esophagus and stomach (with video)," Gastrointest. Endosc. **69**(2), 307–317 (2009).
8. F. J. C. van den Broek, J. B. Reitsma, W. L. Curvers, P. Fockens, and E. Dekker, "Systematic review of narrow-band imaging for the detection and differentiation of neoplastic and nonneoplastic lesions in the colon (with videos)," Gastrointest. Endosc. **69**(1), 124–135 (2009).
9. F. J. C. van den Broek, P. Fockens, S. van Eeden, J. B. Reitsma, J. C. H. Hardwick, P. C. F. Stokkers, and E. Dekker, "Endoscopic tri-modal imaging for surveillance in ulcerative colitis: randomised comparison of high-

#131269 - $15.00 USD Received 7 Jul 2010; revised 17 Aug 2010; accepted 17 Aug 2010; published 19 Aug 2010

resolution endoscopy and autofluorescence imaging for neoplasia detection; and evaluation of narrow-band imaging for classification of lesions," Gut **57**(8), 1083–1089 (2008).
10. J. R. Lakowicz, *Principles of Fluorescence Spectroscopy* (Kluwer Academic / Plenum Publishers, New York, 1999).
11. T. D. Wang, J. M. Crawford, M. S. Feld, Y. Wang, I. Itzkan, and J. Van Dam, "In vivo identification of colonic dysplasia using fluorescence endoscopic imaging," Gastrointest. Endosc. **49**(4), 447–455 (1999).
12. T. Matsuda, Y. Saito, K. I. Fu, T. Uraoka, N. Kobayashi, T. Nakajima, H. Ikehara, Y. Mashimo, T. Shimoda, Y. Murakami, A. Parra-Blanco, T. Fujimori, and D. Saito, "Does autofluorescence imaging videoendoscopy system improve the colonoscopic polyp detection rate?--a pilot study," Am. J. Gastroenterol. **103**(8), 1926–1932 (2008).
13. M. P. L. Bard, A. Amelink, M. Skurichina, M. den Bakker, S. A. Burgers, J. P. van Meerbeeck, R. P. W. Duin, J. G. J. V. Aerts, H. C. Hoogsteden, and H. J. C. M. Sterenborg, "Improving the specificity of fluorescence bronchoscopy for the analysis of neoplastic lesions of the bronchial tree by combination with optical spectroscopy: preliminary communication," Lung Cancer **47**(1), 41–47 (2005).
14. G. W. Falk, "Autofluorescence endoscopy," Gastrointest. Endosc. Clin. N. Am. **19**(2), 209–220 (2009).
15. F. J. C. van den Broek, P. Fockens, S. Van Eeden, M. A. Kara, J. C. H. Hardwick, J. B. Reitsma, and E. Dekker, "Clinical evaluation of endoscopic trimodal imaging for the detection and differentiation of colonic polyps," Clin. Gastroenterol. Hepatol. **7**(3), 288–295 (2009).
16. R. Cubeddu, D. Comelli, C. D'Andrea, P. Taroni, and G. Valentini, "Time-resolved fluorescence imaging in biology and medicine," J. Phys. D Appl. Phys. **35**(9), R61–R76 (2002).
17. H. M. Chen, C. P. Chiang, C. You, T. C. Hsiao, and C. Y. Wang, "Time-resolved autofluorescence spectroscopy for classifying normal and premalignant oral tissues," Lasers Surg. Med. **37**(1), 37–45 (2005).
18. D. B. Tata, M. Foresti, J. Cordero, P. Tomashefsky, M. A. Alfano, and R. R. Alfano, "Fluorescence polarization spectroscopy and time-resolved fluorescence kinetics of native cancerous and normal rat kidney tissues," Biophys. J. **50**(3), 463–469 (1986).
19. L. Marcu, J. A. Jo, P. V. Butte, W. H. Yong, B. K. Pikul, K. L. Black, and R. C. Thompson, "Fluorescence lifetime spectroscopy of glioblastoma multiforme," Photochem. Photobiol. **80**(1), 98–103 (2004).
20. A. Pradhan, B. B. Das, K. M. Yoo, J. Cleary, R. Prudente, E. Celmer, and R. R. Alfano, "Time-resolved UV photoexcited fluorescence kinetics from malignant and non-malignant human breast tissues," Lasers in the Life Sciences **4**, 225–234 (1992).
21. P. A. A. De Beule, C. Dunsby, N. P. Galletly, G. W. Stamp, A. C. Chu, U. Anand, P. Anand, C. D. Benham, A. Naylor, and P. M. W. French, "A hyperspectral fluorescence lifetime probe for skin cancer diagnosis," Rev. Sci. Instrum. **78**(12), 123101 (2007).
22. T. Glanzmann, J.-P. Ballini, H. van den Bergh, and G. Wagnières, "Time-resolved spectrofluorometer for clinical tissue characterization during endoscopy," Rev. Sci. Instrum. **70**(10), 4067–4077 (1999).
23. M. A. Mycek, K. T. Schomacker, and N. S. Nishioka, "Colonic polyp differentiation using time-resolved autofluorescence spectroscopy," Gastrointest. Endosc. **48**(4), 390–394 (1998).
24. S. R. Kantelhardt, J. Leppert, J. Krajewski, N. Petkus, E. Reusche, V. M. Tronnier, G. Hüttmann, and A. Giese, "Imaging of brain and brain tumor specimens by time-resolved multiphoton excitation microscopy ex vivo," Neuro-oncol. **9**(2), 103–112 (2007).
25. R. Cicchi, D. Massi, S. Sestini, P. Carli, V. De Giorgi, T. Lotti, and F. S. Pavone, "Multidimensional non-linear laser imaging of Basal Cell Carcinoma," Opt. Express **15**(16), 10135–10148 (2007).
26. D. S. Elson, N. Galletly, C. Talbot, J. Requejo-Isidro, J. McGinty, C. Dunsby, P. M. P. Lanigan, I. Munro, R. K. P. Benninger, P. De Beule, E. Auksorius, L. Hegyi, A. Sandison, A. Wallace, P. Soutter, M. A. A. Neil, J. Lever, G. W. Stamp, and P. M. W. French, "Mutidimensional fluorescence imaging applied to biological tissue," in *Reviews in Fluorescence 2006*, C. D. Geddes, and J. R. Lakowicz, eds. (Springer Science, New York, 2006), pp. 477–524.
27. P. P. Provenzano, D. R. Inman, K. W. Eliceiri, J. G. Knittel, L. Yan, C. T. Rueden, J. G. White, and P. J. Keely, "Collagen density promotes mammary tumor initiation and progression," BMC Med. **6**(1), 11 (2008).
28. M. C. Skala, K. M. Riching, A. Gendron-Fitzpatrick, J. Eickhoff, K. W. Eliceiri, J. G. White, and N. Ramanujam, "In vivo multiphoton microscopy of NADH and FAD redox states, fluorescence lifetimes, and cellular morphology in precancerous epithelia," Proc. Natl. Acad. Sci. U.S.A. **104**(49), 19494–19499 (2007).
29. E. Dimitrow, I. Riemann, A. Ehlers, M. J. Koehler, J. Norgauer, P. Elsner, K. König, and M. Kaatz, "Spectral fluorescence lifetime detection and selective melanin imaging by multiphoton laser tomography for melanoma diagnosis," Exp. Dermatol. **18**(6), 509–515 (2009).
30. P. I. H. Bastiaens, and A. Squire, "Fluorescence lifetime imaging microscopy: spatial resolution of biochemical processes in the cell," Trends Cell Biol. **9**(2), 48–52 (1999).
31. J. Mizeret, G. Wagnières, T. Stepinac, and H. Bergh, "Endoscopic tissue characterization by frequency-domain fluorescence lifetime imaging (FD-FLIM)," Lasers Med. Sci. **12**(3), 209–217 (1997).
32. Y. Sun, J. Phipps, D. S. Elson, H. Stoy, S. Tinling, J. Meier, B. Poirier, F. S. Chuang, D. G. Farwell, and L. Marcu, "Fluorescence lifetime imaging microscopy: in vivo application to diagnosis of oral carcinoma," Opt. Lett. **34**(13), 2081–2083 (2009).
33. I. Munro, J. McGinty, N. Galletly, J. Requejo-Isidro, P. M. Lanigan, D. S. Elson, C. Dunsby, M. A. Neil, M. J. Lever, G. W. Stamp, and P. M. French, "Toward the clinical application of time-domain fluorescence lifetime imaging," J. Biomed. Opt. **10**(5), 051403 (2005).
34. N. P. Galletly, J. McGinty, C. Dunsby, F. Teixeira, J. Requejo-Isidro, I. Munro, D. S. Elson, M. A. A. Neil, A. C. Chu, P. M. W. French, and G. W. Stamp, "Fluorescence lifetime imaging distinguishes basal cell carcinoma from surrounding uninvolved skin," Br. J. Dermatol. **159**(1), 152–161 (2008).

#131269 - $15.00 USD Received 7 Jul 2010; revised 17 Aug 2010; accepted 17 Aug 2010; published 19 Aug 2010

35. K. Dowling, M. J. Dayel, M. J. Lever, P. M. W. French, J. D. Hares, and A. K. L. Dymoke-Bradshaw, "Fluorescence lifetime imaging with picosecond resolution for biomedical applications," Opt. Lett. **23**(10), 810–812 (1998).
36. H. Schneckenburger, and K. Konig, "Fluorescence Decay Kinetics and Imaging of Nad(P)H and Flavins as Metabolic Indicators," Opt. Eng. **31**(7), 1447–1451 (1992).
37. A. Pradhan, P. Pal, G. Durocher, L. Villeneuve, A. Balassy, F. Babai, L. Gaboury, and L. Blanchard, "Steady state and time-resolved fluorescence properties of metastatic and non-metastatic malignant cells from different species," J. Photochem. Photobiol. B **31**(3), 101–112 (1995).
38. H. D. Vishwasrao, A. A. Heikal, K. A. Kasischke, and W. W. Webb, "Conformational dependence of intracellular NADH on metabolic state revealed by associated fluorescence anisotropy," J. Biol. Chem. **280**(26), 25119–25126 (2005).
39. G. M. Palmer, C. L. Marshek, K. M. Vrotsos, and N. Ramanujam, "Optimal methods for fluorescence and diffuse reflectance measurements of tissue biopsy samples," Lasers Surg. Med. **30**(3), 191–200 (2002).
40. M. Meinhardt, R. Krebs, A. Anders, U. Heinrich, and H. Tronnier, "Wavelength-dependent penetration depths of ultraviolet radiation in human skin," J. Biomed. Opt. **13**(4), 044030 (2008).
41. R. S. Dacosta, B. C. Wilson, and N. E. Marcon, "New optical technologies for earlier endoscopic diagnosis of premalignant gastrointestinal lesions," J. Gastroenterol. Hepatol. **17**(Suppl), S85–S104 (2002).
42. J. Mizeret, T. Stepinac, M. Hansroul, A. Studzinski, H. van den Bergh, and G. Wagnières, "Instrumentation for real-time fluorescence lifetime imaging in endoscopy," Rev. Sci. Instrum. **70**(12), 4689–4701 (1999).
43. A. V. Agronskaia, L. Tertoolen, and H. C. Gerritsen, "High frame rate fluorescence lifetime imaging," J. Phys. D Appl. Phys. **36**(14), 1655–1662 (2003).
44. D. S. Elson, I. Munro, J. Requejo-Isidro, J. McGinty, C. Dunsby, N. Galletly, G. W. Stamp, M. A. A. Neil, M. J. Lever, P. A. Kellett, A. Dymoke-Bradshaw, J. Hares, and P. M. W. French, "Real-time time-domain fluorescence lifetime imaging including single-shot acquisition with a segmented optical image intensifier," N. J. Phys. **6**, 180 (2004).
45. A. Esposito, T. Oggier, H. C. Gerritsen, F. Lustenberger, and F. S. Wouters, "All-solid-state lock-in imaging for wide-field fluorescence lifetime sensing," Opt. Express **13**(24), 9812–9821 (2005).
46. P. J. Tadrous, J. Siegel, P. M. W. French, S. Shousha, N. Lalani, and G. W. H. Stamp, "Fluorescence lifetime imaging of unstained tissues: early results in human breast cancer," J. Pathol. **199**(3), 309–317 (2003).
47. J. Siegel, D. S. Elson, S. E. D. Webb, K. C. Lee, A. Vlandas, G. L. Gambaruto, S. Lévêque-Fort, M. J. Lever, P. J. Tadrous, G. W. H. Stamp, A. L. Wallace, A. Sandison, T. F. Watson, F. Alvarez, and P. M. W. French, "Studying biological tissue with fluorescence lifetime imaging: microscopy, endoscopy, and complex decay profiles," Appl. Opt. **42**(16), 2995–3004 (2003).
48. K. C. Lee, J. Siegel, S. E. D. Webb, S. Lévêque-Fort, M. J. Cole, R. Jones, K. Dowling, M. J. Lever, and P. M. W. French, "Application of the stretched exponential function to fluorescence lifetime imaging," Biophys. J. **81**(3), 1265–1274 (2001).

1. Introduction

Early detection of cancer allows earlier treatment and significantly improves prognosis. While advanced exophytic tumours can usually be visualised, the cellular and tissue perturbations of early neoplasia may not be apparent by direct inspection under white light and are often beyond the discrimination of conventional non-invasive diagnostic imaging techniques. A number of label-free modalities based on the interaction of light with tissue have been proposed to improve the detection of malignant change. These include spectroscopies of various types, including autofluorescence (AF), elastic scattering, Raman, infrared absorption and diffuse reflectance [1–5]. To date, most of these techniques have been limited to point measurements, wherein only a small area of tissue is interrogated, e.g. via a fibre-optic contact probe, at any one time. This enables the acquisition of biochemical information but provides no spatial information about the tissue (i.e. images). Of the spectroscopic imaging techniques, one gaining interest for clinical application is narrow band imaging with reflected light (NBI) [6]. Its clinical utility is still being evaluated [7,8], however, and these instruments often include other contrast techniques such as autofluorescence, in order to obtain further contrast [9]. Autofluorescence provides label-free 'molecular' contrast that can be readily utilised for imaging, allowing the rapid and relatively non-invasive collection of spatially-resolved information from areas of tissue up to tens of centimetres in diameter.

In general, fluorescence may be characterised by the quantum yield of the emitting molecules (fluorophores), by their excitation and emission spectra, by the polarisation state of the emission and by the fluorescence decay rate, which can be parameterised by the fluorescence 'lifetime', i.e. the average time taken to emit fluorescence after excitation from the ground energy level [10]. These spectroscopic properties can vary between different fluorophores and with a fluorophore's local environment. For biological tissue, fluorescence-

#131269 - $15.00 USD Received 7 Jul 2010; revised 17 Aug 2010; accepted 17 Aug 2010; published 19 Aug 2010

based imaging techniques can provide contrast between different types or states of tissue utilizing endogenous tissue fluorophores. In addition, the application of exogenous labels with specific fluorescence properties may be used in order to enhance image contrast. In general, a label-free approach is preferable for clinical imaging, particularly for diagnosis, as it avoids the considerations of toxicity, pharmacokinetics and regulatory approval associated with exogenous agents.

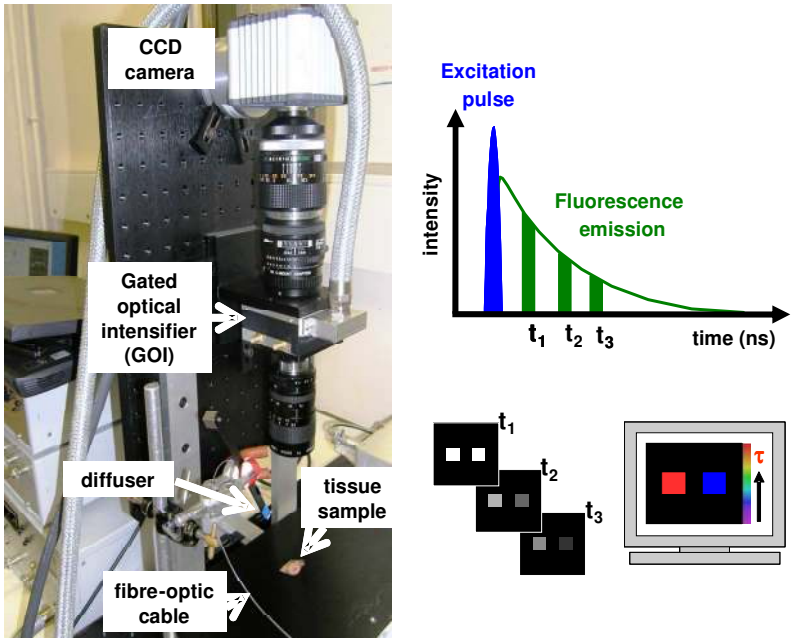

Fig. 1. Equipment set-up for FLIM. The tissue sample is illuminated using a pulsed UV laser source carried via a fibre-optic cable to a diffuser. The emitted autofluorescence is imaged onto the GOI (which acts as a very fast shutter and an intensifier to amplify the weak fluorescence signal) and recorded by the CCD camera. Several time-gated images are recorded at different delays with respect to the excitation pulse. The resulting decay data is then analysed by fitting an exponential decay to the decay for each pixel in the field of view to generate a false-colour lifetime map of the image.

The principal endogenous tissue fluorophores include collagen and elastin crosslinks, reduced nicotinamide adenine dinucleotide (NADH), oxidised flavins (FAD and FMN), lipofuscin, keratin and porphyrins. These fluorophores have excitation maxima in the near-Ultraviolet (UV) or blue/green (325-500 nm) spectral regions. The corresponding fluorescence emission maxima occur at longer (Stokes-shifted) wavelengths in the near-UV to visible (390-700 nm) region of the spectrum [4]. The AF detected from biological tissue will depend on the concentration and quantum yield of the fluorophores present, on the presence of chromophores (principally hemoglobin) that absorb excitation and fluorescence light and on the degree of light scattering that occurs within the tissue [4]. AF signals therefore reflect the biochemical and structural composition of the tissue and so are altered when tissue composition is changed by disease states such as neoplasia.

While clinical endoscopic AF intensity imaging is relatively simple to implement, e.g [11], with a number of systems becoming commercially available, the acquired images may be affected to an unquantifiable extent by variations in a number of factors. These include fluorophore concentration, the temporal and spatial properties of the excitation flux, the angle of the excitation light, the detection efficiency, attenuation by light absorption and scattering within the tissue and spatial variations in the tissue microenvironment that alter local quenching of fluorescence. The use of two or more spectral emission windows can be used to improve quantitation through ratiometric imaging, but the heterogeneity in the distribution of

#131269 - $15.00 USD Received 7 Jul 2010; revised 17 Aug 2010; accepted 17 Aug 2010; published 19 Aug 2010

tissue fluorophores and their broad, strongly overlapping emission spectra limit the degree of discrimination achievable. Although useful AF contrast is obtained in some cases, e.g [9,12], the above considerations have so far limited the widespread use of fluorescence imaging for the detection of malignancy, and current fluorescence imaging tools in clinical use are hampered by low specificity and a high rate of false positive findings [13–15].

Measurements of fluorescence decay profiles depend on relative (rather than absolute) intensity values and fluorescence lifetime imaging (FLIM), for which the fluorescence lifetime is determined for each pixel in a field of view [16], is therefore largely unaffected by many factors that limit steady-state intensity measurements [17]. Fluorescence lifetimes are, however, affected by the transfer of energy from a fluorophore to its surroundings (non-radiative decay) and so FLIM can map changes in local tissue microenvironment (e.g. pH, $[O_2]$, $[Ca^{2+}]$) [10].

The principal tissue fluorophores exhibit characteristic lifetimes ranging from hundreds to thousands of picoseconds and, while changes in kinetics of time-resolved fluorescence between normal versus malignant tissue were reported as early as 1986 [18], the complexity and performance of instrumentation associated with picosecond-resolved measurements, and particularly imaging, have hindered the development of FLIM as a clinical tool. Single point measurements of AF lifetime have, however, revealed differences between normal and neoplastic human tissue *ex vivo* in tumours of brain, breast and skin [19–21]. In addition similar differences have been described *in vivo* in the oral cavity, bladder, oesophagus and lung, and colon [17,22,23].

There have been a few reports of FLIM of AF in cancerous tissues. To date, most have concerned the application of laser scanning microscopes and particularly multiphoton microscopes that inherently incorporate an ultrafast excitation laser and for which the extension to FLIM is readily achieved using commercially available time-correlated single photon counting (TCSPC) electronics. Results obtained using multiphoton FLIM systems to study cancer include *ex vivo* studies of brain, skin, cervix, breast and *in vivo* studies in animals and human skin [24–29]. While laser scanning FLIM microscopy is a powerful approach for cell biology [30], its small field of view (typically less than 1 mm) makes it impractical for imaging the larger areas of tissue interrogation required for many clinical applications such as screening for disease, guided biopsy or intraoperative imaging. This issue, combined with the relatively high cost, is also likely to preclude laser scanning microscopes from many clinical point-of-care applications.

We show here that time-gated FLIM, which may also be performed via an endoscope, can provide label-free contrast with cm-sized fields of view. There have been few applications of AF for imaging cancerous tissue since the first work implemented using a frequency domain FLIM system applied to *ex vivo* bladder and oral mucosa [31], although there has been one recent demonstration of endoscopic FLIM using a pulsed Nitrogen laser source on a hamster model of cancer [32]. Two key factors impeding clinical FLIM instrumentation have been the size, cost and complexity of the excitation lasers and the relatively low signal to noise ratio of the FLIM instrumentation. The recent availability of compact and convenient diode-pumped laser-based UV excitation sources has now addressed the first issue and for the second we have developed efficient time-gated FLIM instrumentation for macroscopic imaging, including through endoscopes [26,33].

Having previously shown that FLIM can distinguish areas of basal cell carcinoma from surrounding skin, we here present results from fresh tissue resections, illustrating, for the first time to our knowledge, the capability to image cancerous tissue in colon, liver and pancreas using FLIM of AF [34]. The apparatus is summarised in Fig. 1 and utilises a compact ultrafast laser excitation source at 355 nm and an optimised detection scheme using a gated optical intensifier read out using a cooled CCD camera.

#131269 - $15.00 USD Received 7 Jul 2010; revised 17 Aug 2010; accepted 17 Aug 2010; published 19 Aug 2010

2. Method

2.1 Sample preparation

Fresh surgical specimens from a number of organs (colon, stomach, bladder, liver, pancreas) were collected from patients undergoing surgical resection for malignant disease. FLIM imaging preceded fixation with formaldehyde. The specimens were either opened (colon, stomach, bladder), cut open (pancreas) or cut into serial slices (liver) by an experienced histopathologist to reveal the malignancy. The specimens were then washed in Hanks' Balanced Salt Solution to remove blood, stool and other debris from the tissue surface, and imaged within 60 minutes of resection. After imaging, the biopsies were photographed and subsequently fixed in formaldehyde. Histological correlation with the photograph and FLIM image, and histopathological analysis was performed by an experienced histopathologist. This study was performed under a protocol approved by the Hammersmith and Queen Charlotte's & Chelsea Hospitals Research Ethics Committee. All patients gave their informed consent to the use of tissue for medical research.

2.2 Fluorescence Imaging Instrumentation and Protocol

Experiments were carried out on a compact FLIM system designed and built by the Photonics Group at Imperial College London and installed in a laboratory space in the Histopathology Department to allow rapid *ex vivo* measurements of the resection specimens immediately after resection. The principles of operation and of the instrumentation used in time-domain FLIM have been described elsewhere [26,35]. In brief, a 10 ps pulsed frequency-tripled Nd:YVO_4 laser (Spectra-Physics Inc, Vanguard 350-HMD355) with an 80 MHz repetition rate provided pulsed UV excitation light at 355 nm. The laser output was delivered to the sample under investigation by a 1 m length of optical fibre (Thorlabs, FT-200-UMT) and a divergent holographic diffuser (Physical Optics Corp, 60° full width half maximum). The emitted fluorescence was imaged via a 375 nm long-pass filter (Schott, GG375) onto a gated optical intensifier (GOI) (Kentech Instruments Ltd, HRI) coupled to a CCD camera (Hamamatsu, ORCA ER) (Fig. 1). The GOI is used to intensify the fluorescence signal and produce ultrashort (1000 ps) time-gated 'snapshots' that are recorded by the CCD camera. By varying the delay between the excitation pulse and the opening of the gated intensifier, images of the exponentially decreasing fluorescence decay were recorded at 25 different time points at 250 ps intervals. A typical decay acquisition took 4 seconds to record. For each sample, 5 decays were acquired sequentially and then averaged to minimise the impact of photobleaching on the lifetime measurement. The total FLIM acquisition time was ~20 s. The CCD camera was also used to record white light reflectance images of the sample under investigation. Image acquisition was controlled by a LabVIEW (National Instruments Corporation, Austin, Texas, USA) program developed in-house by members of the Photonics Group.

2.3 Data processing, lifetime calculation and FLIM map generation

For each pixel in the series of time-gated images, a lifetime value was computed using an iterative weighted non-linear least-squares (WNLLS) algorithm to fit a mono-exponential decay curve to the data. The background signal due to CCD camera readout noise and offset was subtracted prior to fitting. False colour lifetime maps of the specimens were produced by assigning each pixel in the image a colour according to its lifetime value. The fluorescence intensity threshold was adjusted so that signals from outside the specimen were below threshold and excluded from lifetime processing. FLIM maps were also merged with fluorescence integrated intensity images to produce images displaying both lifetime and intensity information. To calculate lifetime values from different regions within the same image, manually delineated region of interest masks were drawn from the white light reflectance images and applied to the processing of the fluorescence decays. All data processing was performed with FLIMProcessing, a LabVIEW program written in-house by members of the Photonics Group.

#131269 - $15.00 USD Received 7 Jul 2010; revised 17 Aug 2010; accepted 17 Aug 2010; published 19 Aug 2010

2.4 Rapid lifetime determination fluorescence lifetime imaging

The method for rapid lifetime determination FLIM has previously been described in detail, see reference [33] and references therein. In brief, a low-jitter electronic delay generator synchronised to the CCD camera's frame grabber status signal was used to adjust the relative delay between time-gated images and allowed the delay to be altered within 2.5 ms. Alternating frames, at delays of 0.2 and 5.7 ns with respect to the excitation pulse, were acquired with an exposure time of 100 ms, resulting in a frame rate of ~7.7 Hz. The detection gate-width was set at 2.4 ns.

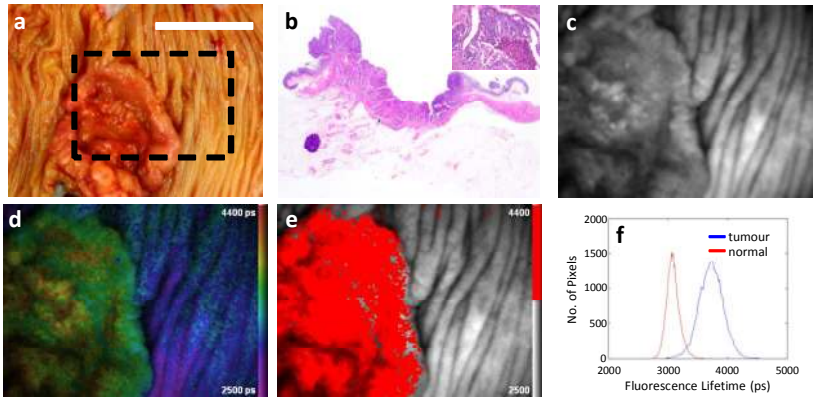

Fig. 2. FLIM of a fresh hemicolectomy specimen containing a moderately differentiated colonic adenocarcinoma. (**a**) White light image of the macroscopic specimen (area of fluorescence imaging outlined). Scale bar (white) represents 2 cm. (**b**) H&E stained histological sections of the tumour. (**c**) Fluorescence integrated intensity image. (**d, e**) Intensity-weighted FLIM images. In (**d**) the lifetime is represented by a continuous spectrum colour scale while in (**e**) it is represented by a binary colour scale. (**f**) Lifetime distribution histograms calculated from the FLIM data.

2.5 Statistical analysis

We compared the mean lifetime and mean intensity values between the paired carcinoma and non-carcinoma regions for each sample with a Wilcoxon Signed-Rank test, as the data is nonparametric. The overlap of distributions of fluorescence intensity or fluorescence lifetime values from carcinoma and non-carcinoma regions for each sample was expressed quantitatively in terms of the area under the curve (AUC) of a receiver operating characteristic curve. The AUC is the probability that the fluorescence intensity/lifetime will correctly identify a randomly selected 'positive' pixel (e.g. presence of cancer) compared to a randomly chosen 'negative' one (e.g. normal tissue). The possible values of AUC therefore run from 0.5, indicating random assignment and therefore no diagnostic use, to either 0 or 1 (depending on the relative position of the histograms) for an ideal indicator.

3. Results

Figure 2 shows fluorescence intensity and FLIM images of a hemicolectomy specimen containing a moderately differentiated colonic adenocarcinoma. The fluorescence lifetimes from the tumour (mean τ = 3730 ps) are longer than those from the normal mucosa (mean τ = 3150 ps) and there is very little contrast between the two regions in the fluorescence intensity images, the FLIM and intensity (not shown) histograms have AUC values of 0.996 and 0.753 respectively. The intensity-weighted FLIM map combines information on the total fluorescence intensity and the fluorescence lifetime and improves the visualization of the sample. Importantly, there is little overlap in the lifetime distributions from the areas of cancer and of the normal mucosa so a binary colour scale, rather than continuous, may be applied, with a cut-off chosen to distinguish between normal and cancerous tissue (in this case 3450 ps). The binary scale would be useful if FLIM of AF was implemented as a clinical 'red-flag'

#131269 - $15.00 USD Received 7 Jul 2010; revised 17 Aug 2010; accepted 17 Aug 2010; published 19 Aug 2010

technique to highlight areas of tumour. Similar lifetime contrast is also observed in gastric cancers and may reflect chemical and morphological changes occurring with malignant change in gastrointestinal mucosa (Fig. 3; mean τ_{cancer} = 2950 ps; mean τ_{normal} = 2510 ps), with an AUC of 0.968.

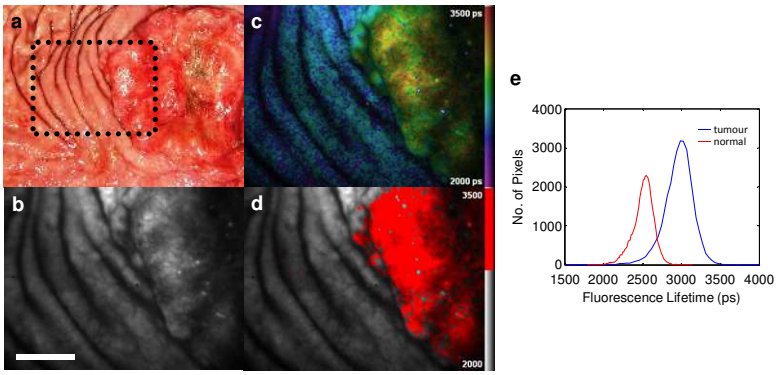

Fig. 3. FLIM of a fresh partial gastrectomy specimen containing a moderately differentiated intestinal-type adenocarcinoma. (**a**) White light image of the macroscopic specimen (area of fluorescence imaging outlined). (**b**) Fluorescence integrated intensity image. Scale bar (white) represents 1 cm. (**c**) Intensity-weighted false-colour FLIM image (lifetime represented by a continuous spectrum colour scale). (**d**) Intensity-weighted false-colour FLIM image (lifetime represented by a discrete binary colour scale). (**e**) Lifetime histogram from the normal and cancerous regions of interest.

Changes in AF fluorescence lifetime are not restricted to glandular mucosa and clear FLIM contrast is seen between squamous cell carcinoma of the bladder and surrounding transitional mucosa (Fig. 4). The contrast is similar to that observed in an earlier study showing a decreased fluorescence lifetime in bladder exhibiting an erythematous urothelium [31]. The asymmetry of the histogram for the tumour ROI in Fig. 4(d) suggests that there may be two or more fluorescent subpopulations within this ROI, however, further work is required to investigate this. In this specific case the fluorescence lifetime discrimination (AUC = 0.878) is not better than that obtained with intensity (AUC = 0.878).

#131269 - $15.00 USD Received 7 Jul 2010; revised 17 Aug 2010; accepted 17 Aug 2010; published 19 Aug 2010

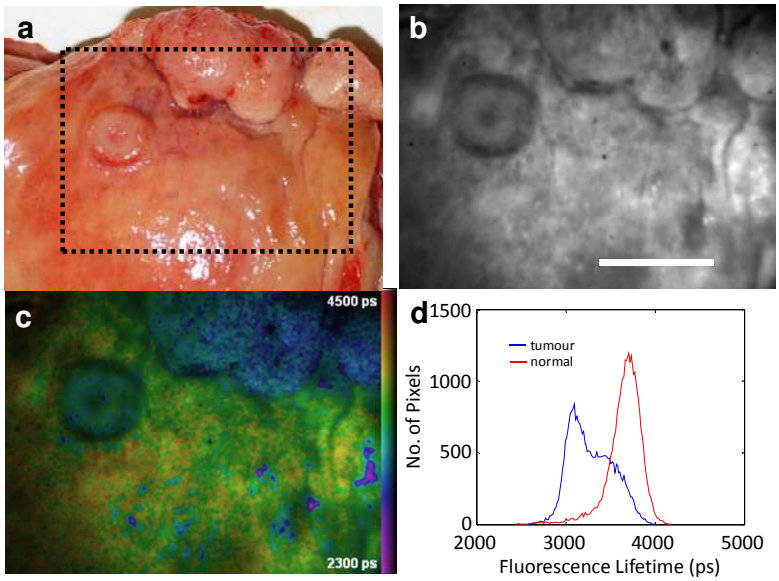

Fig. 4. FLIM of a freshly resected bladder containing a moderately differentiated squamous cell carcinoma. (**a**) White light image of the macroscopic specimen (area of fluorescence imaging outlined). (**b**) Fluorescence integrated intensity image. Scale bar (white) represents 1 cm. (**c**) Intensity-weighted false-colour FLIM image. (**d**) Histogram showing fluorescence lifetime distributions from normal and cancerous regions of interest.

To illustrate the clinical utility of the contrast provided by this FLIM instrument, a series of 18 colonic tumour resections were imaged, of which sixteen were shown by subsequent histopathological analysis to be invasive adenocarcinomas and two were serrated adenomas with focal high grade dysplasia.

To quantify the contrast provided by each FLIM image, two regions of interest (ROI) were defined, one lesional and one uninvolved tissue. A mean fluorescence lifetime was then calculated from the fitted lifetime values for each of the pixels within the ROI. Figure 5(a) shows the difference in mean fluorescence intensity of the lesion compared to the surrounding tissue and 5(b) shows the corresponding difference in fluorescence lifetime. An AUC analysis on the pixel fluorescence intensity [Fig. 5(c)] and lifetime distributions [Fig. 5(d)] from each of the two ROI's for each sample is also presented.

Table 1. Summary of fluorescence data from the 16 imaged adenocarcinomas. Errors are the standard deviation of the values across the 16 specimens. p-values were calculated using a Wilcoxon sign-rank test

n = 16	Fluorescence intensity (a.u.)	Fluorescence lifetime (ps)
Normal	73,000 ± 15,000	3,200 ± 420
Lesion	47,000 ± 12,000	3,700 ± 1,100
Mean difference (lesion-normal)	–26,000 ± 20,000	570 ± 690
p	0.0013	0.0008
Relative change (lesion-normal)/normal	–0.36 ± 0.28	0.18 ± 0.22
Mean AUC	0.20 ± 0.22	0.83 ± 0.22

Interestingly, the two specimens of serrated adenoma (17&18) show a decrease in fluorescence lifetime [Fig. 5(b)] compared to the surrounding tissue, contrary to the trend observed for the cancers (specimens 1-16). These two non-malignant samples have been excluded from the calculation of the average values from all of the carcinoma specimens in the analysis presented in Table 1. Further research is warranted to determine the extent to which this difference in lifetime for the serrated adenoma specimens is significant and to determine the cause.

#131269 - $15.00 USD Received 7 Jul 2010; revised 17 Aug 2010; accepted 17 Aug 2010; published 19 Aug 2010

Samples 13 and 16 also show small decreases in fluorescence lifetime against an overall trend of a longer fluorescence lifetime for tumours. For sample 13, a low AF intensity in the lesional ROI reduced the accuracy of the measured lifetime difference. For sample 16, subsequent histopathology revealed that this specimen consisted of a small (2 mm) region of carcinoma inside a much larger region of adenoma.

Table 1 contains a summary from the fluorescence data acquired from the 16 adenomcarcinomas. The quoted errors are the standard deviation of the values across all specimens. There is a statistically significant contrast between the lesion and normal tissue for both the fluorescence intensity ($p = 0.0013$) and the fluorescence lifetime images ($p = 0.0008$), with the general trend being that the lesions present a decrease in fluorescence intensity and an increase in fluorescence lifetime. The AUC values represent the probability that a randomly chosen pixel in a cancerous region has a greater fluorescence lifetime or fluorescence intensity than a randomly chosen pixel from a non-cancerous region. Therefore, on average, there is an 83% probability that any pixel from a lesion ROI will have a greater fluorescence lifetime and an 80% probability of a lower fluorescence intensity than any pixel from normal tissue. It is important to note that quantitative fluorescence intensity measurements are difficult to perform due to variations in laser intensity, sample illumination, etc, while fluorescence lifetime measurements are not sensitive to these factors. In practice, total intensity values can also be obtained from fluorescence lifetime measurements and therefore both intensity and lifetime data can be used to achieve contrast.

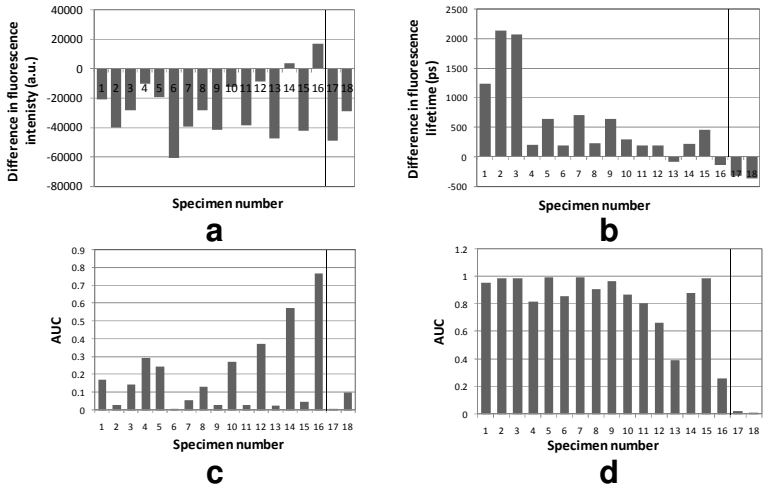

Fig. 5. (a) Graph showing difference in mean fluorescence intensity between the lesion ROI and normal tissue ROI for 18 colonic resections. (b) Plot of the mean difference in fluorescence lifetime between the lesion and normal ROIs. (c) AUC analysis of the fluorescence intensity data. (d) AUC analysis of the fluorescence lifetime data. Specimens 1-16 colonic tumours, 17-18 serrated adenomas.

4. Discussion

In this study, fluorescence was excited at 355 nm, which can excite the majority of tissue fluorophores including collagen crosslinks, NADH, and (to a lesser extent) elastin, oxidised flavins, and porphyrins. In neoplastic change there are a number of factors that would be expected to alter the tissue AF and fluorescence lifetime. These include changes in:

- The metabolic state of cancer cells (e.g. intracellular NADH and flavin concentrations, concentration and fluorescence lifetime of protein-bound NADH) [28,36–38].

#131269 - $15.00 USD Received 7 Jul 2010; revised 17 Aug 2010; accepted 17 Aug 2010; published 19 Aug 2010

- Tissue architecture and morphology (e.g. mucosal expansion displacing submucosal Type I collagen away from the tissue surface; tumour degradation of extracellular matrix or new matrix formation).
- Tissue oxygenation and pH (altered fluorescence lifetime).
- Tissue vascularity (increased light absorption by hemoglobin).
- Nuclear:cytoplasmic ratio in cancer cells (altered light scattering within the tissue).

Samples were imaged within 60 minutes of resection. Although the *ex vivo* AF of fresh biological tissue is similar to that derived from *in vivo* tissue, some physical and metabolic changes will affect AF [39]. Alterations may occur in the amounts of NADH present due to tissue deoxygenation, and hemoglobin content may also change *ex vivo*, altering the absorption properties of the tissue. However, it is likely that any factors that change *ex vivo* tissue fluorescence would affect all areas of a sample to a similar degree and so would be unlikely to artefactually alter the lifetime contrast between normal and neoplastic tissue in *ex vivo* tissue.

FLIM of AF is a potential new clinical imaging technique. UV light has very limited tissue penetration (measured to be typically <1 mm in skin, e.g [40].). Consequently UV light would be unable to excite fluorescence from within solid organs by external illumination. FLIM is therefore limited to cancers from optically accessible tissue surfaces such as the luminal surfaces of the gastrointestinal tract and bladder, and the skin, or during surgery where a non-disturbed cancerous tissue surface is exposed. This paper presents a demonstration that the lifetime of neoplastic tissue AF induced by 355 nm UV excitation may be either shorter (e.g. bladder and pancreatic cancers) or longer (e.g. colonic and gastric adenocarcinoma) than AF from surrounding non-neoplastic tissue. Increased average AF lifetime values have previously been described in oral dysplastic lesions and gliomas by point measurements [17,19], whereas shorter AF lifetime values have been reported in colonic adenomas and esophageal malignancies [23,41]. We note that the point probe AF lifetime measurements of colonic adenoma employed a different excitation wavelength (337 nm) and detection band (530-570 nm) and changes in fluorescence lifetime between normal and malignant tissue have previously been shown to vary depending on emission wavelength [22,23]. Such findings are not surprising given the multiplicity of variables that can alter the lifetime of the AF emitted from neoplastic tissue and highlight the need for further studies to identify the optimum fluorescence imaging parameters for contrasting a given disease and tissue type, including the optimization of the excitation/emission wavelength and possibly the extension to instrumentation employing multiple excitation wavelengths and/or multiple emission channels.

For the *ex vivo* FLIM experiments reported here, we sampled each fluorescence decay profile with 25 time gates and fitted the data to an exponential decay model using an iterative WNLLS algorithm that typically took 10-20 seconds to compute. For maximal clinical utility and ease of use, however, and to minimise the effects of movement artefacts (e.g. from peristalsis), the acquisition and display of fluorescence lifetime images needs to be real-time. Practical real-time FLIM technology could greatly enhance the efficacy of a range of clinical modalities including laparoscopic surgery, gastrointestinal endoscopy (e.g. Barrett's esophagus surveillance, screening for early colonic or gastric neoplasia), colposcopy (e.g. cervical screening), bronchoscopy and cystoscopy.

To demonstrate this potential, we applied a rapid lifetime determination technique, using only two time-gated fluorescence images to produce each lifetime image [33]. FLIM images can thus be updated at up to 10 Hz, which is acceptable for most clinical situations. Figure 6 shows a conventional FLIM image acquired over 20 s alongside a FLIM movie from a series of frames acquired at 7.7 Hz of the same tissue (Media 1). Although the rapidly acquired data exhibits more noise, the lifetime contrast between the cancerous and normal tissue is still apparent. In practice, the apparent noise is reduced when the images are viewed at 7.7 Hz as

#131269 - $15.00 USD Received 7 Jul 2010; revised 17 Aug 2010; accepted 17 Aug 2010; published 19 Aug 2010

the viewer's persistence of vision performs its own integration of the FLIM images. We note that rapidly updated FLIM has been shown to be possible through an endoscope [33,42].

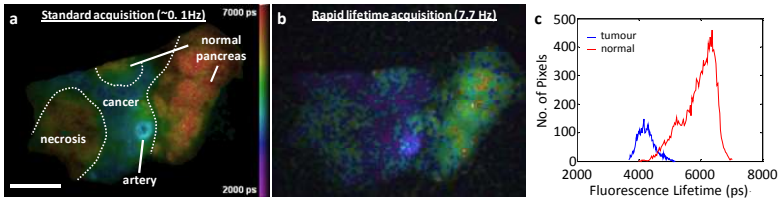

Fig. 6. FLIM of unfixed pancreas containing an area of pancreatic cancer. (**a**) Standard acquisition (25 time gates; decay curve fitted to data using an iterative WNLLS algorithm; update rate ~0.1 Hz). Scale bar (white) represents 5 mm. (**b**) Rapid lifetime determination acquisition (Media 1) update rate 7.7 Hz. (**c**) Histogram of lifetime values from (**A**) showing lifetimes for the cancer and normal regions of interest.

Further increases in FLIM imaging rates may be achieved using "single-shot" techniques utilising image splitting optics in combination with an optical delay line or segmented GOI, to realise simultaneous acquisition of up to four time-gated images [43,44]. In the longer term, the development of modulated CMOS technology may result in compact and cost-effective solid-state time-resolved detectors that could ultimately be miniaturised and deployed at the distal end of FLIM endoscopes, removing the need to transmit images through a fibre imaging bundle [45].

The measurement of fluorescence lifetimes in biological tissue is complicated by the presence of multiple fluorophores that exist in a range of different microenvironments [10]. As a result, the fluorescence decays are generally complex. Although they do not fit precisely to a single exponential decay profile, in practice they can be approximated to this model, returning an average fluorescence lifetime. This has been used previously for FLIM of biological tissue AF and been shown to generate lifetime contrast between different types and states of tissue [26,34,46] and allows the rapid acquisition/processing necessary for a clinically useful imaging tool.

More complex decay models, for example double or triple exponentials, would provide better fits and have been used when analysing lifetime data of biological tissue AF. This improved fit, however, is often only the result of the higher number of fitting parameters used; it is no more realistic to assume the presence of only 2 or 3 mono-exponentially decaying fluorophores (or a single fluorophore with 2 or 3 discrete decay constants) in each pixel of the entire FLIM map than it is to assume the presence of a single fluorophore [47]. Fitting multi-exponential decays is more vulnerable to noise artefacts and requires significantly longer acquisition and computation time compared with fitting a single exponential decay curve to the data.

Despite the lifetime values generated in our FLIM maps being an approximation to the complex nature of the fluorescence decay and the absolute lifetime values, clear meaningful contrast between normal tissue and neoplasia is still obtained and the potential for FLIM endoscopy is clear. However, if the AF signal is sufficiently strong so as to allow complex exponential fitting, then it clearly provides additional opportunities to contrast different types and states of tissue. This is demonstrated in Fig. 7, which shows a 10 mm thick slice through a right trisegmentectomy liver resection containing a large metastatic adenocarcinoma from a colonic primary. A margin of paler tissue representing radiofrequency ablation (RFA) thermal injury can be seen along the bottom edge of the specimen in the white light image.

Although the fluorescence signal from the area of RFA injury and normal liver can be distinguished on the basis of the single exponential fit [Fig. 7(c)], it is not possible to contrast normal and tumour tissue in this case. Interestingly, all three regions are clearly contrasted when performing a stretched exponential fit [Fig. 7(d)–7(f)] [48]. Both the stretched exponential fluorescence lifetime and heterogeneity fit parameter (a measure of the lifetime distribution in a pixel) provide contrast between all three regions. This data highlights the

#131269 - $15.00 USD Received 7 Jul 2010; revised 17 Aug 2010; accepted 17 Aug 2010; published 19 Aug 2010

potential of more complex fluorescence decay analysis to provide further contrast between different types and states of tissue when sufficient fluorescence signal can be obtained.

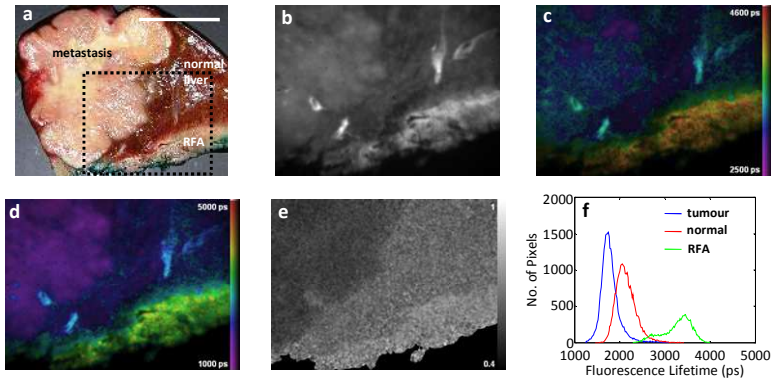

Fig. 7. FLIM of an unfixed liver containing metastatic colorectal carcinoma and an area of radiofrequency ablation damage. (**a**) White light image of the specimen (area of fluorescence imaging indicated by rectangle). Scale bar (white) represents 2 cm. (**b**) Fluorescence intensity image. (**c**) FLIM map obtained with a single exponential fit. (**d**) Stretched exponential FLIM map and (**e**) heterogeneity images obtained with a stretched exponential fit. (**f**) Lifetime histogram generated from the stretched exponential fit demonstrating contrast between the three areas of the sample.

5. Conclusion

The use of FLIM of tissue AF to aid the detection and delineation of neoplastic change is an emerging concept. To date, the complexity of imaging picosecond-resolved time-gated AF has precluded the clinical exploitation of this valuable source of tissue contrast. To our knowledge this is the first study of FLIM applied to mucosal carcinomas and the first report of practical FLIM instrumentation that uses robust all-solid state laser technology. In addition, we have demonstrated the potential of FLIM for extended wide-field imaging providing cm-sized fields of view of liver, gastric, bladder and pancreatic cancer.

We believe that FLIM has significant potential clinical value as a label-free imaging modality to quickly screen tissue and detect small cancers and pre-cancerous lesions that are not immediately apparent to the naked eye. The wide-field nature of this imaging modality allows the comparative display of healthy tissue surrounding 'abnormal' tissue, and hence its role is envisaged as a 'red flag' guide to potential areas of malignancy, reducing time and the number of screening biopsies taken. In addition, FLIM could be a tool for delineating areas of malignancy and enhancing the identification of tumour margins. This would be useful preoperatively in judging the required extent of surgical resections or the application of ablative therapies.

Further studies will be necessary to optimise and refine the technique to maximise the contrast available for a given tissue or tumour and these promising early findings should be replicated *in vivo*. Future work will also include an investigation of FLIM contrast in earlier disease states, e.g. precancerous tissue, and in more subtle disease states, e.g. flat dysplasia, than was possible with the surgical resection specimens that were available for this study. However, it is already apparent that lifetime imaging adds a useful additional dimension of contrast to fluorescence instrumentation and that the clinical application of FLIM for the detection and delineation of malignancy is now feasible and informative.

Acknowledgements

The assistance of the Human Biomaterials Resource Centre of Imperial College Healthcare NHS Trust in obtaining tissue for this study is gratefully acknowledged. The authors gratefully acknowledge a Beacon Award (QCBB/C/012/0007C) from the UK Department of

Trade and Industry and a research grant from the Engineering and Physical Sciences Research Council (EP/F040202/1). Paul French acknowledges a Royal Society Wolfson Research Merit Award.

#131269 - $15.00 USD Received 7 Jul 2010; revised 17 Aug 2010; accepted 17 Aug 2010; published 19 Aug 2010